Multipole response of metal spheres to q-dependent excitation operators

Llorenç Serra, Francesca Garcias, and Manuel Barranco
Departament de Física, Universitat de les Illes Balears, E-07071 Palma de Mallorca, Spain

Nuria Barberán
Departament d'Estructura i Constituents de la Matèria, Universitat de Barcelona, E-08028 Barcelona, Spain

Jesús Navarro
Departament de Física Atòmica, Molecular i Nuclear e Instituto de Física Corpuscular del Consejo Superior de Investigaciones Científicas, Universitat de València, Burjassot, E-46100, València, Spain

(Received 17 July 1989)

We have obtained the once and thrice energy-weighted moments of the random-phase-approximation (RPA) response to q-dependent excitation operators of type $j_L(qr)Y_{L0}$ for metal spheres described within a spherical jellium model. These two moments, in conjunction with the Thomas-Fermi estimation of the RPA inverse energy-weighted moment, are used to study the response of these systems as a function of q. For small values of q, we recover the surface-mode systematics, whereas for large q's the response is mainly determined by electron-hole excitations. For intermediate q values, bulk oscillations are found and their connection with the hydrodynamical-mode predictions is established. In the limit of a big sphere, we have obtained an improved bulk-plasmon pole approximation for the dispersion relation which includes in a very easy way exchange and correlation effects. We have found that these corrections are not negligible. The moments of the response corresponding to a plane wave $e^{i\mathbf{q}\cdot\mathbf{r}}$ are also discussed. Numerical applications to the case of Na spheres whose ground-state structure is described by models of different complexity (constant electronic density, Thomas-Fermi or Kohn-Sham) are presented.

I. INTRODUCTION

A considerable amount of work has been recently devoted to the study of the response of metal clusters to electromagnetic fields, and especially to the characterization of surface collective excitations (see, for example, Refs. 1–8 and references therein). For small clusters, the increasing surface-to-volume ratio has suggested that the response would be dominated by surface-type excitations. However, recent electron-energy-loss-spectroscopy experiments on metallic spheres[9] have shown that, contrary to what was expected, significant bulk scattering occurs even on 50-Å diam spheres.

Bulk collective excitations of metallic spheres have been theoretically described using a nonlocal dielectric function,[7] a hydrodynamical model,[4,10] and a self-consistent time-dependent local-density approximation.[11]

Recently, some of us have carried out rather detailed random-phase-approximation (RPA) sum-rules (SR) calculations of the response (strength) function to multipole operators $r^L Y_{L0}$, where Y_{L0} is the spherical harmonic function, that generate surface collective oscillations on these spheres.[8,12] In spite of the fact that the method only gives an average picture of the strength, a great deal of information could be obtained from a careful examination of the numerical results.

To explore the nonlocal response of the system, in the present work we extend our previous calculations[8,12] to q- and L-dependent operators of the kind $j_L(qr)Y_{L0}$, where $j_L(qr)$ is the spherical Bessel function of order L. We will see that this operator generates bulk as well as surface and electron-hole excitations in different proportions depending on the value of q. Thus, selecting the appropriate q, information about bulk collective modes can be extracted and compared with the predictions of other models.

As in Refs. 8 and 12, we employ the spherical-jellium model to describe the neutralizing positive background. The valence-electron cloud of the unperturbed cluster is described either in the Kohn-Sham (KS) or in an improved Thomas-Fermi–vonWeizsäcker (ITFW) plus a local-density approximation (Dirac-Wigner) for the exchange and correlation effects.

This paper is organized as follows. The RPA sum rules m_1 and m_3 pertaining to the operator $j_L(qr)Y_{L0}$ are deduced in Sec. II. In Sec. III we use the ITFW method of Ref. 12 to obtain the m_{-1} SR. The numerical results corresponding to $j_L(qr)Y_{L0}$ are presented in Sec. IV. In Sec. V, the preceding results are employed to obtain m_{-1}, m_1, and m_3 for the plane-wave operator $e^{i\mathbf{q}\cdot\mathbf{r}}$, and in Sec. VI we draw our conclusions. Finally, we present in the Appendix the exact expressions of m_1 and m_3 for $j_L(qr)Y_{L0}$ corresponding to a constant ground-state (g.s.) electron density.

II. RPA SUM RULES

A. General description

RPA sum rules are described in detail in Refs. 13 and 14 (see Refs. 8, 12, 15, and 16 for applications to metal

clusters). Here, we just recall the definitions and fundamental results we shall use in this paper.

Sum rules m_k are moments of the strength function

$$S(E)=\sum_n \delta(E-E_n)|\langle n|Q|\phi\rangle|^2 , \tag{1}$$

where the sum (integral in the case of continuum spectrum) extends over all the excited states of the system. Q is the external field acting on the system; E_n, $|n\rangle$, and $|\phi\rangle$ are the excitation energies, the excited states, and the g.s. of the system, respectively. By definition

$$m_k=\int E^k S(E)dE=\sum_n E_n^k|\langle n|Q|\phi\rangle|^2 . \tag{2}$$

The mean energy $\bar{E}$ and the variance σ^2 read

$$\begin{aligned}&\bar{E}=m_1/m_0 ,\\ &\sigma^2=m_2/m_0-(m_1/m_0)^2 .\end{aligned} \tag{3}$$

Among these moments, the ones with $k=-1$, 1, and 3 play an important role in the application of SR to the study of collective resonance states of the system. First of all, they can be obtained *with RPA precision* from Kohn-Sham calculations, essentially involving g.s. expectation values. Secondly, they can be used to estimate $\bar{E}$ and σ^2. Indeed, defining $E_k=(m_k/m_{k-2})^{1/2}$ it has been shown[13] that

$$\begin{aligned}&E_1\le\bar{E}\le E_3 ,\\ &\sigma^2\le(E_3^2-E_1^2)/4 .\end{aligned} \tag{4}$$

If most of the strength is in a narrow energy region, as is the case for some resonance states, E_1 and E_3 are good estimates of $\bar{E}$. Conversely, if E_1 and E_3 are close, we may infer that some strength is concentrated around these values.

The inverse energy-weighted SR

$$m_{-1}=\sum_n \frac{1}{E_n}|\langle n|Q|\phi\rangle|^2 \tag{5}$$

is closely related to the static polarizability α, $\alpha=2m_{-1}$. It can be obtained from constrained KS calculations. Indeed, solving in the KS approximation the problem

$$H+\lambda Q , \tag{6}$$

where λ is a (small) constraining parameter, it is possible to show[13] that m_{-1} RPA may be evaluated as

$$m_{-1}=-\frac{1}{2}\frac{d\langle Q\rangle_\lambda}{d\lambda}\bigg|_{\lambda=0}=\frac{1}{2}\frac{d^2\langle H\rangle_\lambda}{d\lambda^2}\bigg|_{\lambda=0} . \tag{7}$$

m_1 and m_3 RPA can be obtained as expectation values on the KS g.s. $|\phi\rangle$ of suitable operators. For Hermitian operators Q we have[13]

$$m_1=\tfrac{1}{2}\langle\phi|[Q,[H,Q]]|\phi\rangle , \tag{8a}$$

$$m_3=\tfrac{1}{2}\langle\phi|[[H,[H,Q]],[H,Q]]|\phi\rangle . \tag{8b}$$

The linear energy-weighted SR is easily evaluated from Eq. (8a) when Q only depends on the position. The cubic energy-weighted SR is easier to obtain by scaling $|\phi\rangle$. Defining the scaled many-electron wave function

$$|\phi_\eta\rangle=e^{\eta[H,Q]}|\phi\rangle \tag{9}$$

we get

$$m_3=\frac{1}{2}\frac{\partial^2}{\partial\eta^2}\langle\phi_\eta|H|\phi_\eta\rangle\,\Big|_{\eta=0} . \tag{10}$$

If $[H,Q]$ is a one-electron operator $|\phi_\eta\rangle$ is still a Slater determinant and m_3 is obtained with RPA precision. We define the scaled particle and kinetic-energy densities

$$\begin{aligned}&n_\eta(\mathbf{r})=\langle\phi_\eta|\hat{n}|\phi_\eta\rangle=n+\eta n_1+\eta^2 n_2+\cdots ,\\ &\tau_\eta(\mathbf{r})=\langle\phi_\eta|\hat{\tau}|\phi_\eta\rangle=\tau+\eta\tau_1+\eta^2\tau_2+\cdots ,\end{aligned} \tag{11}$$

where

$$\begin{aligned}&\hat{n}=\sum_i \delta(\mathbf{r}-\mathbf{r}_i) ,\\ &\hat{\tau}=\sum_i \overleftarrow{\nabla}_i\delta(\mathbf{r}-\mathbf{r}_i)\vec{\nabla}_i ,\end{aligned} \tag{12}$$

and

$$\begin{aligned}&n=\langle\phi|\hat{n}|\phi\rangle ,\\ &n_1=\langle\phi|[\hat{n},[H,Q]]|\phi\rangle ,\\ &n_2=\tfrac{1}{2}\langle\phi|[[\hat{n},[H,Q]],[H,Q]]|\phi\rangle ,\end{aligned} \tag{13}$$

with similar expressions for τ, τ_1, and τ_2. Notice that our particle, and kinetic-energy densities are defined as

$$\begin{aligned}&n=\sum_i |\phi_i|^2 ,\\ &\tau=\sum_i |\nabla\phi_i|^2 .\end{aligned}$$

Developing the expectation value (10) in powers of η, the above expressions alow for a straightforward (but) cumbersome) evaluation of m_3.

General expressions for n_1, n_2, τ_1, and τ_2 have been recently obtained.[17] For velocity-independent potentials and r-dependent operators Q, which is our case, one can show[17] that τ_1 does not contribute to m_3 and that

$$n_1=-\hbar\vec{\nabla}(n\mathbf{u})=-\hbar\nabla^i(nu^i) , \tag{14}$$

$$n_2=-\tfrac{1}{2}\hbar\vec{\nabla}(n_1\mathbf{u})=-\tfrac{1}{2}\hbar\nabla^i(n_1u^i) , \tag{15}$$

$$\begin{aligned}\tau_2=&\tfrac{1}{3}\tau\{-u^k(\nabla^k\nabla^i u^i)+(\nabla^j u^i)[\nabla^i u^j+\nabla^j u^i]\}+\tfrac{1}{4}(\nabla^i\nabla^j u^j)[\nabla^i\nabla^k(nu^k)]\\ &+\tfrac{1}{4}(\nabla^i n)(\nabla^j\nabla^k u^k)[\nabla^i u^j+\nabla^j u^i]+\tfrac{1}{2}(2\tau-3\lambda)[S_{ik}(\nabla^j u^k)(\nabla^i u^j+\nabla^j u^i)-u^k S_{ij}(\nabla^i\nabla^k u^j)] ,\end{aligned} \tag{16}$$

where ∇^i means the Cartesian i-coordinate derivative and a sum over repeated indices is understood. $\mathbf{u}$ is the collective velocity field

$$\mathbf{u}=\frac{\hbar}{m}\vec{\nabla}Q \ , \tag{17}$$

S_{ij} is the second-rank symmetric tensor

$$S_{ij}=\frac{x_i x_j}{r^2}-\tfrac{1}{3}\delta_{ij} \ , \tag{18}$$

and $\lambda(r)$ is the "centrifugal" kinetic-energy density

$$\lambda(r)=\frac{1}{4\pi r^2}\sum_\alpha 2(2l_\alpha+1)l_\alpha(l_\alpha+1)\frac{|\varphi_\alpha(r)|^2}{r^2} \ , \tag{19}$$

where $\varphi_\alpha(r)/r$ is the one-electron radial wave function. In the $\hbar^0$ Thomas-Fermi (TF) approximation one has $\lambda=2\tau/3$. We refer the interested reader to Refs. 17–19 for further details.

B. m_1 and m_3 for $j_L(qr)Y_{L0}$ operators

As in Ref. 8, we have considered an electron-energy density functional consisting of a kinetic term (T), a Coulomb direct term (E_c), a Coulomb exchange term of Slater type (E_{cx})

$$E_{cx}=-\frac{3}{4}\left[\frac{3}{\pi}\right]^{1/3}\int d\mathbf{r}[n(r)]^{4/3}\equiv\int d\mathbf{r}\,\varepsilon_{cx}(r) \ , \tag{20}$$

a correlation term of Wigner type ($E_{\rm corr}$)

$$E_{\rm corr}=-a\int d\mathbf{r}\frac{n(r)}{b+r_s(n)}\equiv\int d\mathbf{r}\,\varepsilon_{\rm corr}(r) \ , \tag{21}$$

where $r_s(n)=[3/4\pi n(r)]^{1/3}$ is the *local* radius per electron, and a jellium-jellium term $[E_{jj}=\frac{3}{5}(Ne)^2/R]$ and a jellium-electron term (E_{je})

$$E_{je}=\int d\mathbf{r}\,V_j(r)n(r) \ , \tag{22}$$

where $V_j(r)$ is the jellium Coulomb potential and R is the radius of the jellium sphere. A direct evaluation of Eq. (8a) yields

$$\begin{aligned} m_1&=\frac{\hbar^2}{2m}\int d\mathbf{r}(\vec{\nabla}Q)^2n(r) \\ &=\frac{\hbar^2}{2m}\int_0^\infty dr\,r^2\left[(j')^2+\frac{L(L+1)}{r^2}j^2\right]n(r) \ , \end{aligned} \tag{23}$$

where $n(r)$ is the g.s. unperturbed KS electron density, j is a short notation for $j_L(qr)$, and j' denotes the r derivative of $j_L(qr)$.

The evaluation of m_3 is straightforward, but tedious. We have repeatedly used that

$$\Delta[j_L(qr)Y_{L0}]=-q^2j_L(qr)Y_{L0} \ .$$

For electron-density terms, like E_{cx} or $E_{\rm corr}$, we get

$$\begin{aligned} m_3(cx,\ \text{corr})&=-\frac{\hbar^2}{2m}\int d\mathbf{r}\,\varepsilon_2(n)n_1(r)\Delta Q \\ &=-\frac{1}{2}\left[\frac{\hbar^2}{m}\right]^2\int_0^\infty dr\,r^2\varepsilon_2(n)q^2jg(r) \ , \end{aligned} \tag{24}$$

where we have defined

$$g(r)\equiv n'j'-q^2nj$$

and

$$\varepsilon_2(n)\equiv n\frac{\partial^2\varepsilon}{\partial n^2} \ .$$

Thus, for the Coulomb exchange term we have

$$\varepsilon_2(n)=-\frac{1}{3}\left[\frac{3}{\pi}\right]^{1/3}n^{1/3}\equiv\varepsilon_2^{cx}(n) \ , \tag{25}$$

and for the correlation term

$$\varepsilon_2(n)=-\frac{2a}{9}r_s(n)\frac{b+2r_s(n)}{[b+r_s(n)]^3}\equiv\varepsilon_2^{\rm corr}(n) \ . \tag{26}$$

(In all the formulas, a prime will denote the r derivative, and Δ the Laplacian of the corresponding function.)

The kinetic contribution reads

$$\begin{aligned} m_3(T)=\frac{1}{2}\left[\frac{\hbar^2}{m}\right]^3\Bigg[\int_0^\infty dr\Bigg\{&[\tfrac{1}{2}r^2(\Delta\lambda+3\lambda q^2+\tfrac{1}{2}\Delta nq^2)-\Phi(r)-\tfrac{1}{2}r^2\Delta\Phi(r)-r\Phi'(r)]\left[(j')^2+\frac{L(L+1)}{r^2}j^2\right] \\ &+3\Phi(r)\left[r^2(j'')^2+L(L+1)\left[\frac{j^2}{r^2}+(j')^2-\frac{2}{r}jj'\right]\right]\Bigg\}-\tfrac{1}{4}q^4\int_0^\infty dr\,r^2jg(r)\Bigg] \ , \end{aligned} \tag{27}$$

where we have defined $\Phi(r)=\tau-3\lambda/2$. In the $\hbar^0$ TF approximation, $m_3(T)$ is considerably simplified by the fact that $\lambda=2\tau/3$.

The electron-electron (e-e) and jellium-electron (j-e) Coulomb contributions are

$$m_3(e\text{-}e)=2\pi e^2\left[\frac{\hbar^2}{m}\right]^2\left[\frac{2}{2L+1}\int_0^\infty\frac{1}{r^{L-1}}g(r)dr\int_0^r r_1^{L+2}g(r_1)dr_1+\int_0^\infty g(r)j'dr\int_0^r n(r_1)r_1^2\,dr_1\right] \ , \tag{28}$$

$$m_3(j\text{-}e)=-2\pi e^2\left[\frac{\hbar^2}{m}\right]^2\int_0^\infty g(r)j'\,dr\int_0^r n_J(r_1)r_1^2\,dr_1 \ , \tag{29}$$

where

$$n_J(r)=n^+\theta(R-r) \tag{30}$$

with $R=r_sN^{1/3}$, r_s being the radius per valence electron of the bulk monovalent metal, N the number of atoms in the sphere, and n^+ the positive background density, $n^+=3/4\pi r_s^3$. We will refer to the sum $m_3(j\text{-}e)+m_3(e\text{-}e)$ as $m_3(C)$.

Equations (23)–(29) are the sought after ones for m_1 and m_3. It is important to realize that they only depend on the particle and kinetic-energy densities (and on some of their r derivatives) of the *unperturbed* sphere. Consequently, both sum rules can be obtained with RPA precision by numerical quadrature after carrying out a rather simple KS calculation.

The simple structure of Eqs. (23)–(29) offers the possibility of obtaining accurate numerical estimates of m_1 and m_3 RPA by semiclassical models, provided that they yield good g.s. densities, as is discussed in Ref. 8. It would have been wrong, however, to start from a TF energy density functional and then to perform the scaling indicated by Eq. (9). In particular, the basic kinetic-energy contribution to m_3, Eq. (27), would have been missing. A detailed discussion of this point can be found in Ref. 20.

For $L\neq 0$, in the limit $q\to 0$ we recover the expressions derived in Ref. 8 for surface modes. Indeed, since

$$j_L(qr)\sim\frac{(qr)^L}{(2L+1)!!}\quad\text{as } q\to 0\ ,$$

the operator $j_L(qr)Y_{L0}$ is proportional to r^LY_{L0} when $q\to 0$. It is easy to check that, apart from the overall factor $[q^L/(2L+1)!!]^2$, Eqs. (24)–(29) reduce to the ones derived in Ref. 8. Notice in particular that if $\Delta Q=0$, as it is for $Q=r^LY_{L0}$, m_3 has no explicit contribution from exchange and correlation energies in the local-density approximation, see Eq. (24). These energies do influence m_3 through self-consistency because they play some role in the determination of the g.s. densities $n(r)$, $\tau(r)$, and $\lambda(r)$.

III. m_{-1} FOR $j_L(qr)Y_{L0}$ OPERATORS

To solve the constrained KS problem, Eq. (6), is a formidable task because in almost all cases of practical interest, the external field breaks the spherical symmetry of the unperturbed sphere. However, in contradistinction with the m_3 case already discussed, the TF model can be used to obtain good estimates of m_{-1} (Refs. 12, 14, and 16) provided, of course, it is able to reproduce fairly well the global properties of the unperturbed sphere. To this end, we have used the following ITFW energy density functional (in atomic units):

$$\varepsilon(n)=\tfrac{1}{2}\gamma n^{5/3}+\tfrac{1}{8}\beta\frac{(\nabla n)^2}{n}-C_xn^{4/3}-\frac{an}{b+r_s(n)}+\tfrac{1}{2}\int\frac{n(\mathbf{r})n(\mathbf{r}')}{|\mathbf{r}-\mathbf{r}'|}d\mathbf{r}'+V_jn\ , \tag{31}$$

where $\gamma=3/5(3\pi^2)^{2/3}$, $C_x=3/4(3/\pi)^{1/3}$, $a=0.44$ and $b=7.8$, and V_j is the jellium Coulomb potential

$$V_j=\begin{cases}\dfrac{2\pi}{3}n^+r^2-2\pi R^2n^+, & r\le R\\ -\dfrac{N}{r}=-\dfrac{4\pi}{3}R^3\dfrac{n^+}{r}, & r\ge R\ .\end{cases}$$

The value of the coefficient β in Eq. (31) has been fixed so as to reproduce the RPA E_3 energies corresponding to r^LY_{L0} operators.[8,12] For Na spheres, its optimum value is 0.5.[12]

To obtain m_{-1} in the ITFW approximation, we have solved the constrained problem

$$E[n]=\int d\mathbf{r}\,\varepsilon(n)+\lambda\int d\mathbf{r}\,Qn(\mathbf{r})\ , \tag{32}$$

where $Q=j_L(qr)Y_{L0}$, and λ is a small parameter. In order to find the equilibrium density $n(\mathbf{r})$, one has to solve the Euler-Lagrange equation

$$\frac{\delta\varepsilon(n)}{\delta n}+\lambda j_L(qr)Y_{L0}=\mu\ , \tag{33}$$

where μ is the chemical potential. Since we are interested only in λ^1-order changes in $n(\mathbf{r})$ with respect to the unconstrained equilibrium density [that will be called $n_0(r)$ in this section to avoid misunderstanding], we can write without loss of generality

$$n(\mathbf{r})=n_0(r)+\delta n(\mathbf{r})\equiv n_0(r)+\lambda f(r)Y_{L0} \tag{34}$$

with $f(r)$ an unknown function that depends on L and q. Substituting Eq. (34) into Eq. (33) and using the equilibrium condition for $\lambda=0$

$$\frac{\delta\varepsilon(n_0)}{\delta n_0}=\mu\ , \tag{35}$$

we get the following integro-differential equation for $f(r)$:

$$-\frac{\beta}{4}\frac{d^2f}{dr^2}+\frac{\beta}{4}\left[-\frac{2}{r}+\frac{n_0'}{n_0}\right]\frac{df}{dr}+\left\{\frac{\beta}{4}\left[\frac{L(L+1)}{r^2}+\frac{\Delta n_0}{n_0}-\left[\frac{n_0'}{n_0}\right]^2\right]+\tfrac{5}{9}\gamma n_0^{2/3}+\varepsilon_2^{ex}(n_0)+\varepsilon_2^{corr}(n_0)\right\}f$$
$$+n_0j_L(qr)+\frac{4\pi}{2L+1}\left[\frac{n_0}{r^{L+1}}\int_0^r dr_1\,r_1^{L+2}f(r_1)+n_0r^L\int_r^\infty dr_1\frac{f(r_1)}{r_1^{L-1}}\right]=0\ . \tag{36}$$

After determining $f(r)$ we have

$$\langle Q\rangle_\lambda=\int d\mathbf{r}\,j_L(qr)Y_{L0}n(\mathbf{r})=\int d\mathbf{r}\,j_L(qr)Y_{L0}\delta n(\mathbf{r})\ .$$

Thus,

$$m_{-1}=-\tfrac{1}{2}\int_0^\infty dr\,j_L(qr)r^2f(r)\ . \tag{37}$$

Equation (36) has been solved in Ref. 12 for r^LY_{L0} operators. We refer the reader to this reference for more de-

tails concerning the ITFW method and the practical solution of that equation, as well as a discussion of the properties of its solutions.

A technical question arises for the operator $j_0(qr)Y_{00}$. In this case, the condition

$$\int \delta n(\mathbf{r})d\mathbf{r}=0$$

is not automatically fulfilled. Put it in a different way, the chemical potentials μ in Eqs. (33) and (35) are not identical to first order in λ and the right-hand side of Eq. (33) has to be written as $\mu+\lambda\delta\mu$. Correspondingly, the right-hand side of Eq. (36) is $n_0\delta\mu$ instead of zero, and one has to iterate on the unknown $\delta\mu$ to enforce particle-number conservation.

IV. RESULTS FOR $j_L(qr)Y_{L0}$ OPERATORS

A. Finite spheres

We have applied the method described in the preceding sections to Na spheres for which we have taken $r_s=4$ a.u. [we shall use atomic units (a.u.) in the numerical applications]. Figures 1–3 show for Na_{92} and $L=0$, 1, and 5, the contribution to m_3(RPA) of the different terms entering its definition, Eqs. (24)–(29). Each contribution has been normalized dividing it by the total m_3. We stress again that to obtain m_3(RPA), we have used in Eqs. (24)–(29) the KS g.s. densities $n(r)$, $\tau(r)$, and $\lambda(r)$.

These figures show that for small values of q, we recover the behavior corresponding to surface modes:[8] For small L values, m_3 is dominated by the (j-e) and (e-e) Coulomb contributions. The local Coulomb exchange (cx) and correlation (corr) contributions are small and negative, the latter contribution being always negligible.

Coulomb (C) and kinetic (T) contributions equalize at a value of q close to $q_c=\omega_p/v_F=0.45$ a.u., where $\omega_p=(4\pi ne^2/m)^{1/2}=0.217$ a.u. is the plasma frequency and

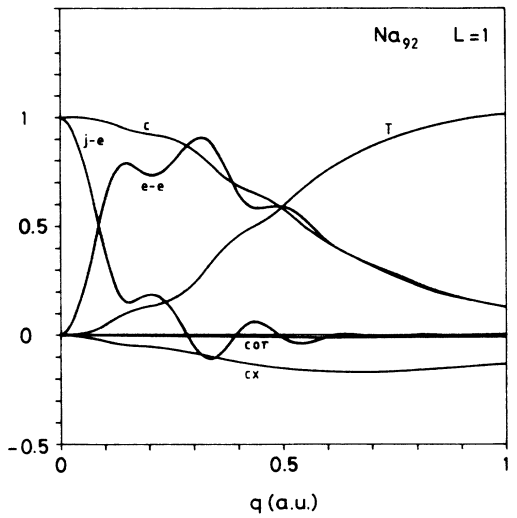

FIG. 2. Same as Fig. 1 for Na_{92} $L=1$.

$v_F=\hbar q_F/m=\hbar(3\pi^2n)^{1/3}/m=0.48$ a.u. is the Fermi velocity. For larger q values, m_3 is eventually determined by the kinetic contribution.

This cutoff q_c is a lower bound approximation to the Landau damping onset momentum. The transition from a collective to a single electron-hole excitation is related to the increasing contribution of the kinetic energy to m_3 for large values of q and independently, for large values of L as can be seen form Fig. 3. That was already shown in the case of surface oscillations in Ref. 8, where following a similar reasoning, it was found an upper bound of the critical angular momentum for which collective excitations can be sustained by a given sphere.

Figures 4–9 collect the basic numerical results of this work. We have represented there the ITFW E_1 and E_3

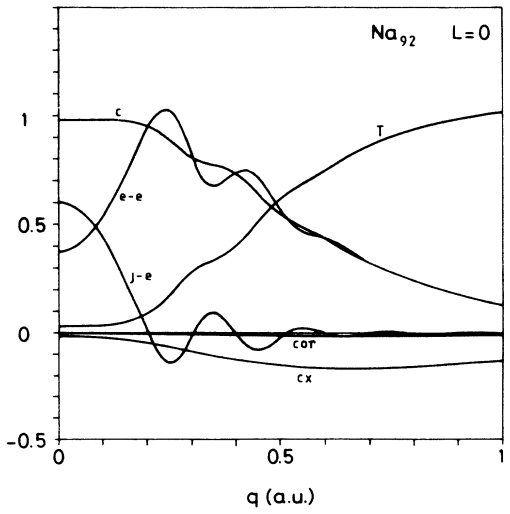

FIG. 1. q dependence of the m_3 (RPA) relative contributions of the different terms entering its definition [Eqs. (24)–(29)] for the case Na_{92} $L=0$.

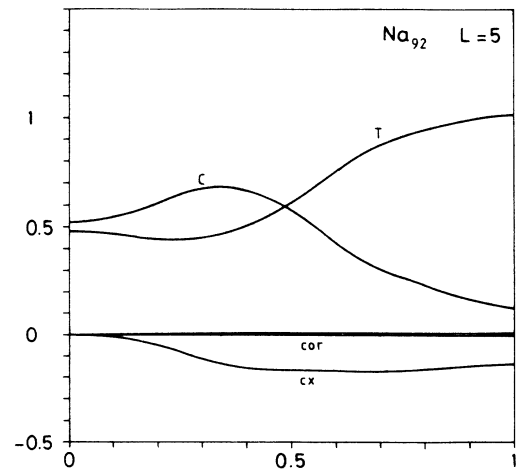

FIG. 3. Similar to Fig. 1 for Na_{92} $L=5$.

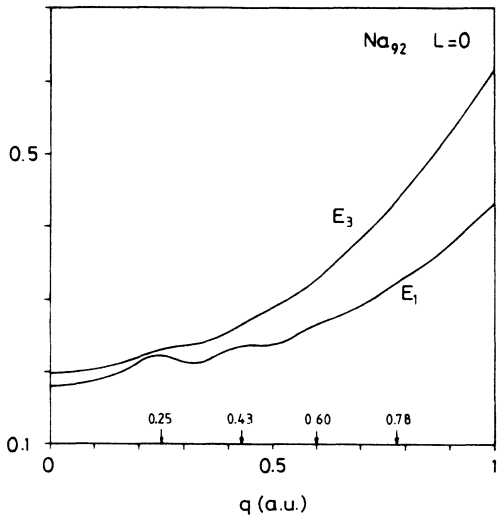

FIG. 4. Na_{92} E_1 and E_3 ITFW energies vs q for $L=0$. The arrows indicate the first four roots of Eq. (38). All the quantities are in atomic units.

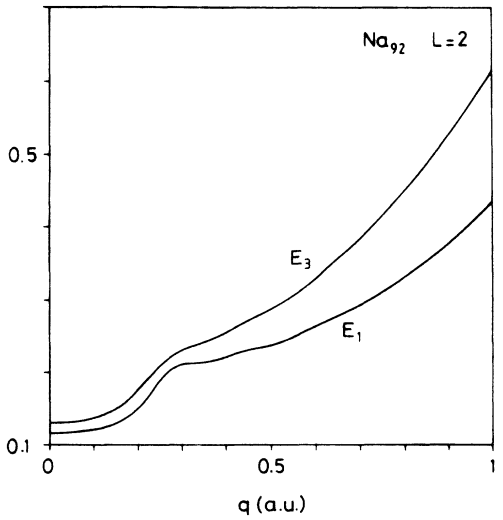

FIG. 6. Same as Fig 4 for Na_{92} $L=2$.

energies (solid lines) corresponding to the Na_{92} $L=0-5$ modes. These energies have been calculated from the m_{-1} obtained according to the method of Sec. III and from Eqs. (23)–(29) of Sec. II, putting $\Phi(r)=0$ in Eq. (27) and using the ITFW densities $n(r)$, $\tau(r)$, and $\lambda(r)$, i.e., *after* m_1 and m_3 have been deduced in the RPA framework, as we have indicated at the end of Sec. II. Let us comment on the more salient features of these figures.

One can first observe that the difference between E_3 and E_1 increases when q increases; the electron-hole (noncollective) contribution becomes the main excitation mechanism for values of $q \geq q_c$.

Apart from $L=0$, all the other modes have a region at small values of q for which E_1 and E_3 are rather q independent, tending to the $q=0$ surface-mode value. This means first, that the excitation is mainly of surface type and second, that the energy of the *single* (one for each L value) surface modes obtained in Ref. 8 for the step electron-density model,

$$\hbar^2\omega^2=\hbar^2\omega_p^2\frac{L}{2L+1}+\tfrac{2}{3}\hbar^2(2L+1)(L-1)\frac{\beta_F^2}{R^2}\ ,$$

where $\beta_F=(\frac{3}{5})^{1/2}v_F$, *has no extra q-dependent correction term.* For Na_{92}, the surface-dominated region extends up to $q\sim 0.1$ for $L=1$ and up to $q\sim 0.2$ for $L=5$. After this flat region (which is absent in the $L=0$ mode), the response starts being dominated by bulk modes, and both energies increase rapidly.

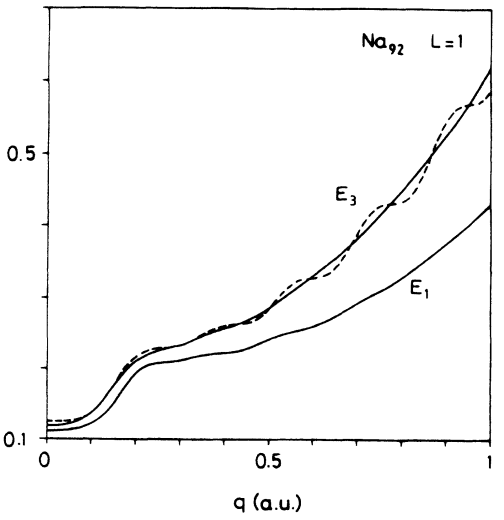

FIG. 5. Same as Fig. 4 for Na_{92} $L=1$. The dashed line is the result corresponding to the step-electron-density model.

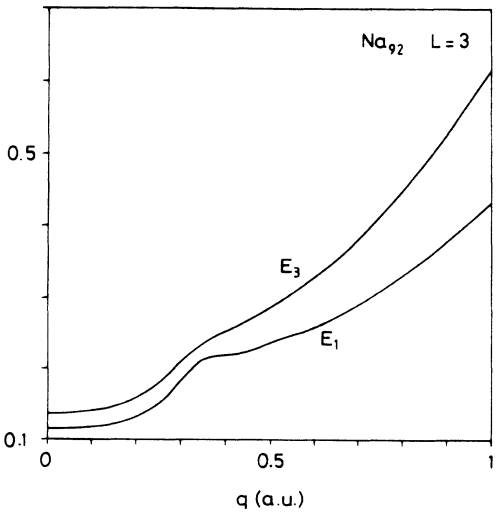

FIG. 7. Same as Fig. 4 for Na_{92} $L=3$.

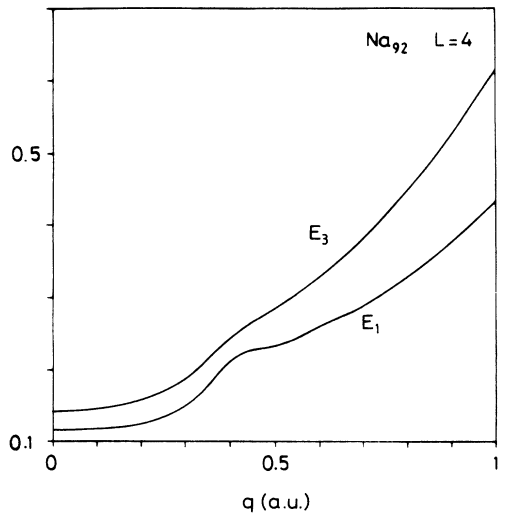

FIG. 8. Same as Fig. 4 for Na_{92} $L=4$.

To give an idea about how these results depend on the ITFW approximation, for E_3 $L=5$, we show in Fig. 9 the TF result, i.e., the result obtained using in the RPA expressions the ITFW densities, as well as the full RPA result obtained using in the RPA expressions the KS densities. One can see that the agreement between both calculations is excellent (see also Refs. 8 and 12). For smaller values of L, barely can one tell the difference between both models.

It is also worth noting the structures along the E_1 curves which are also present in the E_3 curves, although less marked. They are clearly visible along the $L=0$ E_1 curve (Fig. 4). The maxima of these structures correspond to the q-quantized bulk modes in the hydrodynamical approximation. Indeed, for a constant g.s. electron density, these modes are excited at discrete values of q such that[4]

$$j_{L+1}(qR)=0 \ . \tag{38}$$

[Actually, Eq. (38) is exact only for $L=0$ modes; for $L \gg 1$ it is a good approximation[4].] In Fig. 4 we have indicated by arrows the first four roots of Eq. (38) corresponding to $R \sim 18.06$, which is the Na_{92} jellium radius. To a good approximation, it is also the equivalent sharp radius of its valence-electron density R_e defined as

$$R_e^2=\tfrac{5}{3}\langle r^2\rangle \ ,$$

where

$$\langle r^2\rangle=\frac{1}{N}\int d\mathbf{r}\, r^2 n(r) \ .$$

For Na_{92} we have $R_e \sim 18.29$. The agreement between the values of q furnished by the hydrodynamical model and the ones corresponding to the maxima is remarkable (see also Ref. 11), allowing us to interpret these structures as bulk modes which are preferentially excited at selected values of q.

It is also interesting to observe in Fig. 4 that E_1 and E_3 get very close at the first volume mode. This gives a hint about its collectiveness, which is more pronounced than for the other $L=0$ bulk modes.

For $q > q_c$ and all L values, the spectrum is dominated by electron-hole excitations. The energy and momentum are so large that the excited electron is quasifree, and its dispersion relation is $\sim q^2/2$. This parabolic behavior is a common feature of Figs. 4–9.

In the case of $L=0$, we also have a bulk mode at $q=0$ that can be excited by the operator $Q=r^2$ (Ref. 8). Its energy usually lies above the energy of the surface modes, tending to ω_p when the radius of the sphere goes to infinity. For $L \geq 1$, the $q=0$ mode is of surface type and its associated induced electron density is peaked at the surface. Indeed, when $q \to 0$ we have from Eq. (14)

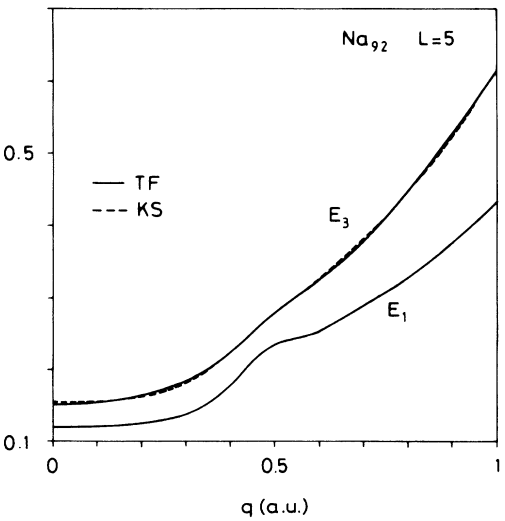

FIG. 9. Same as Fig. 4 for Na_{92} $L=5$. The dashed line is the full RPA result obtained from KS densities.

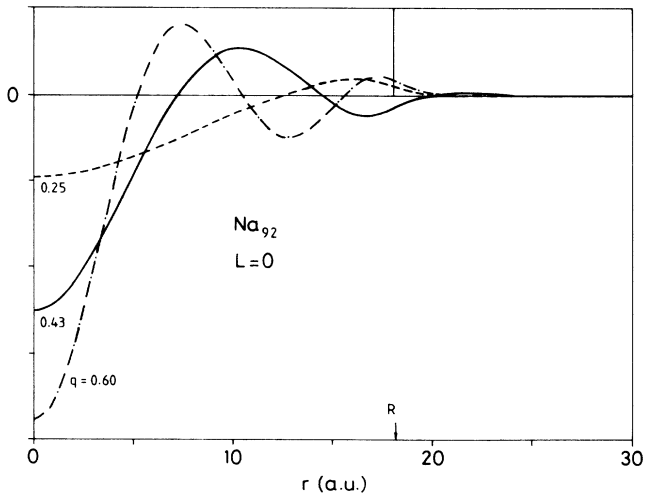

FIG. 10. Induced electronic-density functions (in arbitrary units) corresponding to the first three E_1 local maxima displayed in Fig. 4. The vertical line and arrow labeled R show the position of the jellium surface.

$$n_1 = -\frac{\hbar^2}{m}\vec{\nabla}(n\vec{\nabla}Q) \sim n'(r) r^{L-1} Y_{L0} .$$

The induced electron-density functions $f(r)$ defined in Eq. (34) which correspond to the first three maxima of $E_1(L=0)$ are displayed in Fig. 10 in arbitrary units. The position of the jellium surface is indicated by a vertical line and an arrow labeled R. The number of nodes increases by one from q_i to q_{i+1}, as in the hydrodynamical model. The last node of each density is located at almost the same r value ($\sim$20 a.u.). For the $L=0$, $q=0$ mode generated by $Q=r^2$, $f(r)$ is similar (but not identical) to the m_3-induced density $n_1 \sim 3n_0(r)+rn_0'(r)$.[8] It has only one node at $r \sim 17.2$ a.u.

A better understanding of the E_1, and E_3 maxima can be obtained from the q behavior of m_{-1}, m_1, and m_3 which is displayed in Fig. 11 for Na_{92} $L=0$, and in Fig. 12 for $L=1$ and 5 (notice the different scales for the three sum rules). From these figures we see that m_{-1} has the strongest structure and that the peaks in E_1 and E_3 are partially washed out by the slightly out-of-phase character of the structures along the m_{-1} and m_1 curves.

Remarkable is the constancy of m_1 for $q \geq q_c$ and also that above q_c the SR are rather L independent, as can be seen from Fig. 12 and especially from a detailed comparison of Figs. 11 and 12. The behavior of m_1 and m_3 as a function of q and L can be investigated using a step-electron-density model which has the advantage of yielding analytical (but involved) expressions for these SR. The exact expressions for m_1 and m_3 corresponding to this model are given in the Appendix. They have been straightforwardly obtained from Eqs. (23)–(29) taking for n a constant density equal to the jellium one, Eq. (30).

The dashed line in Fig. 5 represents the E_3 energy obtained with the step-electron-density model for Na_{92} and $L=1$. We see that the step-density model nicely follows the trend of the exact RPA calculation. Only for small values of q is the difference (in relative value) appreciable because surface modes demand a good description of the surface.[8]

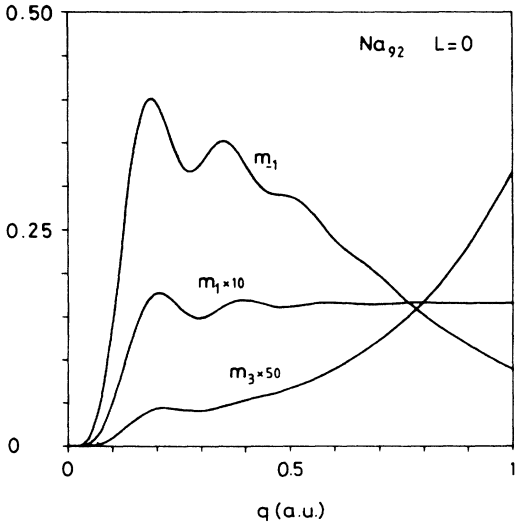

FIG. 11. Na_{92} m_{-1}, m_1, and m_3, sum rules (in a.u.) for $L=0$.

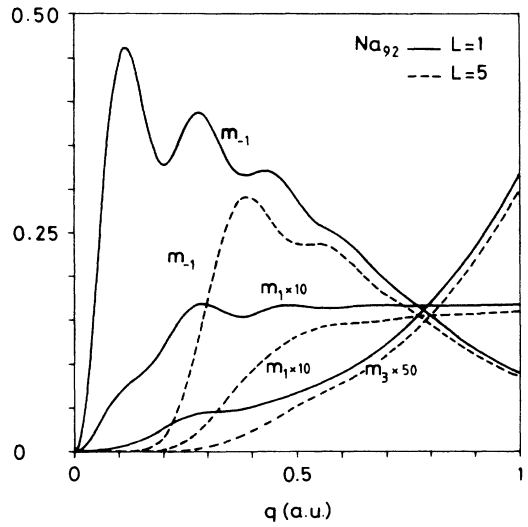

FIG. 12. Same as Fig. 11 for Na_{92} $L=1$ (solid line) and $L=5$ (dashed line).

Taking the q and/or $R \to \infty$ limit of Eqs. (A1)–(A4), one gets the following asymptotic formulas:

$$m_1 = \frac{\hbar^2}{4m} nR , \tag{39}$$

$$m_3 = \left[\frac{\hbar^2}{m}\right]^2 \frac{R}{4}\left[4\pi e^2 n^2 + n\left[\frac{\hbar^2}{m}\gamma n^{2/3} + \varepsilon_2^{cx}(n) + \varepsilon_2^{corr}(n)\right]q^2 + \frac{\hbar^2}{4m} n q^4\right] , \tag{40}$$

where $n = n^+ = 3/4\pi r_s^3$, the quantities $\varepsilon_2^{cx}(n)$ and $\varepsilon_2^{corr}(n)$ have been defined in Eqs. (25) and (26), and γ is after Eq. (31).

These formulas not only explain the qualitative behavior of m_1 and m_3 shown in Figs. 11 and 12, but also yield values for these SR in quantitative agreement with the exact results for $q \geq q_c$ that can be easily checked in the case of m_1. For the step-density model and $q \leq 1$, we have not reached the asymptotic region yet. This is clear if one remembers the oscillatory behavior of E_3 (step) shown in Fig. 5. The jellium radius of Na_{92}, $R \sim 18$ is too small for making $qR \gg 1$ if $q \leq 1$. However, the use of a realistic model in which the electronic density goes to zero exponentially, like TF or KS, makes the asymptotic formulas (39) and (40) valid just above $q \geq 0.5$ because the finite size quantization effects are not as strong as in the step-electronic-density model. That can also be seen in Fig. 13, where we have plotted E_3 versus q for Na_{196} for $L=0$ to 5. The nonoscillatory behavior and L independence predicted by the ratio m_3/m_1 determined from Eqs. (39) and (40) is apparent. Another feature clearly visible in Fig. 13 is the displacement of the first volume

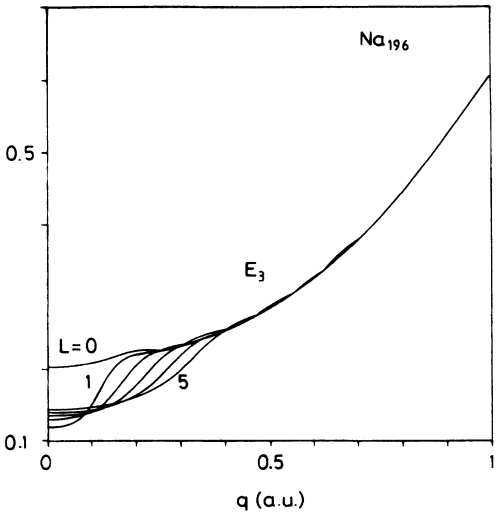

FIG. 13. Na_{196} ITFW E_3 energies (in a.u.) for $L=0-5$.

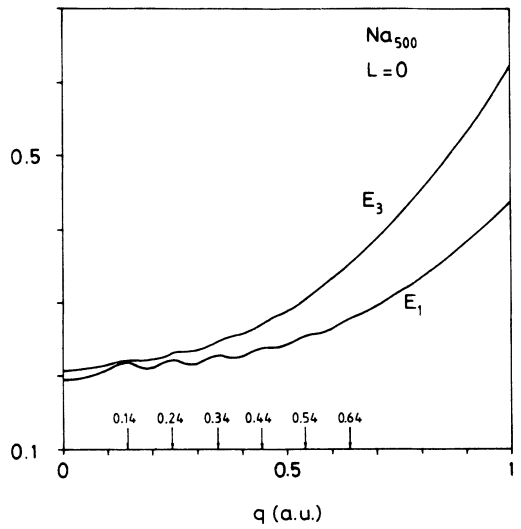

FIG. 15. Same as Fig. 4 for Na_{500}.

peak to higher values of q when L increases. That can also be seen from Figs. 4–9, and it is in qualitative agreement with the results of the hydrodynamical model [see Eq. (38)].

For a given sphere, the number of volume modes of L type that can be excited with appreciable strength, i.e., the number of maxima along the E curves, depends on how many of the selected values of q given approximately by Eq. (38) can be found before the corresponding excitation energy lies in the electron-hole strongly damped excitation region. For small spheres, the first bulk L mode occurs at a rather high q because R is small. Thus, although their electron shell structure is such that the typical electron-hole energies are large, only one harmonic is appreciably excited because the second one already has $q \sim q_c$. This is illustrated for Na_{20} $L=0$ in Fig. 14. For large spheres, the first bulk L mode lies at a rather small q and consequently, there is room enough to accommodate many harmonics before $q \geq q_c$. However, since the electron-hole energies are also small for large spheres, it might well happen that, for a given L, the high-order harmonics will also be strongly damped. This is not completely so in our model, as can be observed from Fig. 15, where we have plotted the results corresponding to Na_{500} $L=0$. The number of peaks has increased with respect to the Na_{20} and Na_{92} cases. As in Figs. 4 and 14, we have indicated the position of the first bulk modes predicted by the hydrodynamical model. Notice again how close E_1 and E_3 are at the first maximum. The structures we find along the E_1 and E_3 curves in our ITFW model have been confirmed in a full RPA calculation using the KS densities.[21] For $q \sim q_c$, E_1(KS) is lower than E_1(TF) by about 10%, whereas E_3(KS)$\approx E_3$(TF) as we have already shown in Fig. 9.

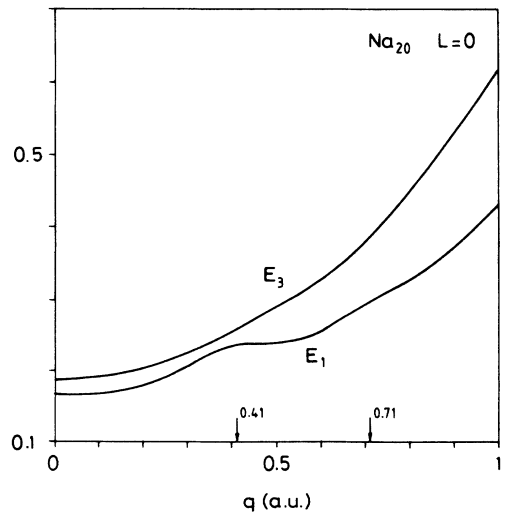

FIG. 14. Same as Fig. 4 for Na_{20}.

Figure 16 shows the E_1 and E_3 Na_{92} average energies at the first (q_1) bulk mode as a function of L. For completeness, we also show the $L=0$, $q=0$ mode value (lower triangle and dot points at $L=0$). We have the general trend already obtained in Ref. 7 using a nonlocal dielectric function and also in Ref. 4 using the hydrodynamical model. The only significant difference between our results and those of Refs. 4 and 7 is the existence of a minimum in $E(L)$ at $L=1$. We attribute the existence of this minimum to the contribution of the low-energy surface L mode to the *average*. This effect is more marked for $L=1$ since the corresponding surface energy is the smallest. Very likely, it is also present in all the other L modes. This is not a surface-diffuseness effect; indeed, we have found a similar result using the step-density model.

Figure 17 shows the E_1 and E_3 energies versus N for $L=0$ and 1 corresponding to the first maximum q_1. For small spheres, the location of the $L=1$ maximum is rather uncertain and this is the reason for the error bars, which have been roughly estimated. We have not found any convincing explanation of the $L=1$, E_1, curve.

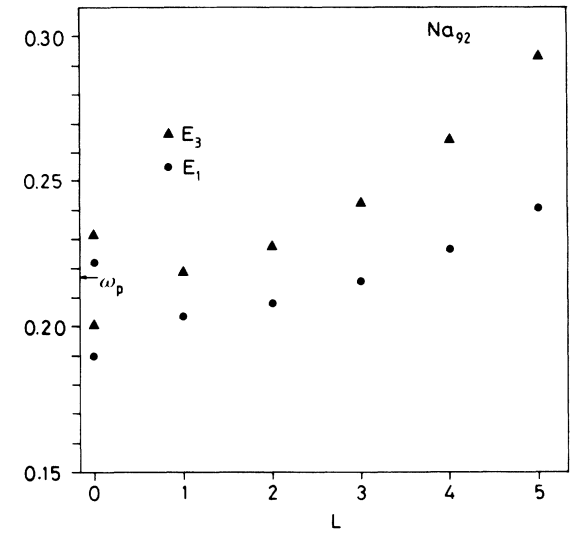

FIG. 16. Na_{92} E_1 and E_3 energies (in a.u.) as functions of L, corresponding to the q_1 bulk mode. For $L=0$, the lower circle and triangle represent the $q=0$ mode. The arrow labeled ω_p indicates the plasma energy.

Apart from it, the E_3 energies show the proper decreasing behavior with N of the hydrodynamical mode.[4]

B. Infinite systems

Let us come back to Eqs. (39) and (40). Introducing the plasma frequency ω_p and the Fermi velocity v_F we have (in atomic units)

$$\omega^2 \equiv \frac{m_3}{m_1} = \omega_p^2 + \left[\frac{3}{5} v_F^2 - \frac{v_F}{3\pi} + \varepsilon_2^{\text{corr}} \right] q^2 + \frac{q^4}{4} , \quad (41)$$

where the term $-v_F/3\pi$ is just the local exchange contribution ε_2^{ex}. This formula is a generalization of the dispersion relation for bulk modes of an infinite metal given by the plasmon-pole approximation for the electron-gas

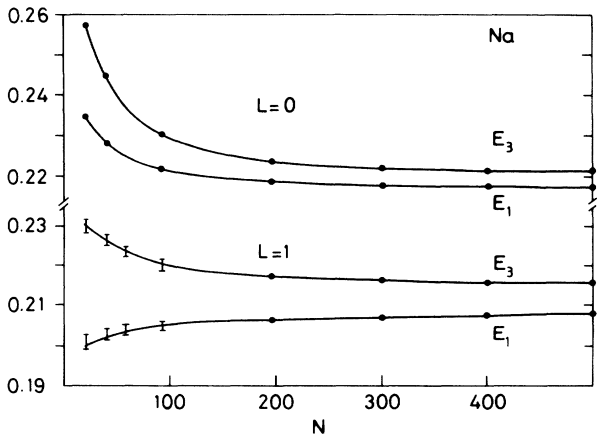

FIG. 17. q_1-bulk-mode E_1 and E_3 energies (in a.u.) for Na spheres of different numbers of atoms. The upper curves correspond to $L=0$ and the lower curves to $L=1$.

response.[22] To our knowledge, Eq. (41) has not been previously obtained. We would like to emphasize that it has been derived with RPA precision within the spherical-jellium model and that the basic approximations we have made are first, to neglect electron surface diffuseness and second, to consider the limit of a large-radius sphere.

It is interesting to estimate the contribution of the kinetic, Coulomb exchange, and correlation energies to the q^2 term in Eq. (41) (the q^4 term has a pure kinetic origin). Using for a and b the values given after Eq. (31), we have that for $r_s=4$, the kinetic, exchange, and correlation energy contributions are 0.138, -0.051, and -0.004. Thus, altogether exchange and correlation are 40% of the q^2 kinetic-energy contribution. For Al ($r_s=2$) the corresponding figures are 0.552, -0.102, and -0.002. In this case, the correction is of 20%. We conclude that these contributions (Coulomb exchange mostly) are important and should be taken into account.

V. THE m_{-1}, m_1, and m_3 MOMENTS FOR THE PLANE-WAVE OPERATOR $e^{i\mathbf{q}\cdot\mathbf{r}}$

It is straightforward to obtain the m_{-1}, m_1, and m_3 moments for the operator $e^{i\mathbf{q}\cdot\mathbf{r}}$ from the previous results. If one is not interested in the incident direction, averaging on the q angles, one has

$$m_k = \int \frac{d\hat{\mathbf{q}}}{4\pi} \sum_n E_n^k |\langle n | e^{i\mathbf{q}\cdot\mathbf{r}} | \phi \rangle|^2 , \quad (42)$$

where $\hat{\mathbf{q}}$ is a unit vector in the $\mathbf{q}$ direction. Using the expansion

$$e^{i\mathbf{q}\cdot\mathbf{r}} = 4\pi \sum_{LM} i^L j_L(qr) Y_{LM}^*(\hat{\mathbf{q}}) Y_{LM}(\hat{\mathbf{r}})$$

and the imposed spherical symmetry of $|\phi\rangle$, we get

$$m_k = \sum_L 4\pi(2L+1) \sum_n E_n^k |\langle n | j_L(qr) Y_{L0} | \phi \rangle|^2 . \quad (43)$$

Thus,

$$m_k(e_{av}^{i\mathbf{q}\cdot\mathbf{r}}) = \sum_{L=0}^{\infty} 4\pi(2L+1) m_k(j_L(qr) Y_{L0}) . \quad (44)$$

For m_1 it is again easy to find a compact expression in the case of $Q = e^{i\mathbf{q}\cdot\mathbf{r}}$, although some attention has to be paid to the fact that Q is not Hermitian. For non-Hermitian operators, Eq. (8.1) becomes

$$m_1 = \tfrac{1}{2} \langle \phi | (Q^+ [H, Q] - [H, Q^+] Q) | \phi \rangle \quad (45)$$

and due to the angular averaging,

$$m_1 = \int \frac{d\hat{\mathbf{q}}}{4\pi} \frac{1}{2} \langle \phi | [Q^+, [H, Q]] | \phi \rangle . \quad (46)$$

For the plane wave, it reduces to

$$m_1 = \int \frac{d\hat{\mathbf{q}}}{4\pi} \frac{\hbar^2}{2m} \int d\mathbf{r}\, n(r) (\nabla e^{-i\mathbf{q}\cdot\mathbf{r}}) (\nabla e^{i\mathbf{q}\cdot\mathbf{r}}) = \frac{\hbar^2 q^2}{2m} N . \quad (47)$$

This exact result has been used to test the convergence of the series (44). We have summed it to guarantee a 0.1% precision on m_1 and have checked that a similar

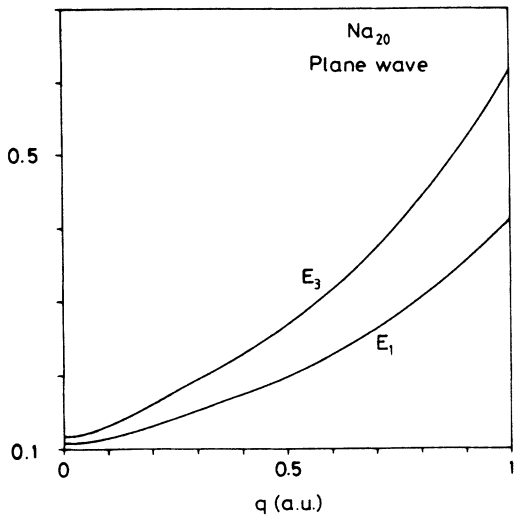

FIG. 18. Na_{20} E_1 and E_3 energies (in a.u.) corresponding to a plane-wave operator.

precision is achieved on m_{-1} and m_3. The number of terms to consider in Eq. (44) depends on the values of q and N. For Na_{92} and $q=1$, 22 terms are needed to have a 0.1% precision in the three sum rules, whereas for $q=0.3$, eight terms are enough.

We represent in Figs. 18 and 19 the plane-wave results for Na_{20} and Na_{1000}, respectively. Two salient features are worth commenting upon. The first one is the presence of a flat region for small q values in the Na_{20} case that has almost disappeared for Na_{1000}. This behavior is related to the impossibility for photons (represented by plane waves) to excite surface modes on infinite plane surfaces, whereas for nonplanar geometries, and in particular for small spheres, the probability of exciting surface modes by real photons is not zero.

The second feature is that the response in the bulk-mode region is dominated by the dipole $L=1$ mode, which is typical of light-absorption processes.[3] That can be seen from Fig. 19, where the rise in the E_1 and E_3 curves is at the position of q_1 ($L=1$), which is indicated by an arrow.

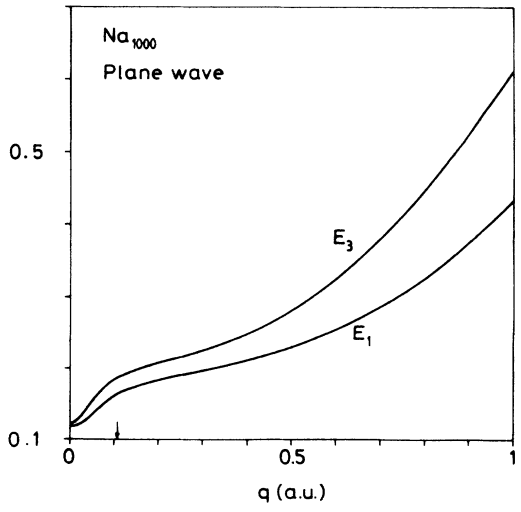

FIG. 19. Same as Fig. 18 for Na_{1000}. The arrow indicates the first q value for which $j_2(qR)=0$.

VI. DISCUSSION AND CONCLUDING REMARKS

We have studied the response of metallic spheres to q- and L-dependent operators $j_L(qr)Y_{L0}$. The RPA sum-rules technique has permitted us to obtain the average excitation energies of surface and bulk modes of these systems.

One of the main advantages of our method is that only electron ground-state quantities are needed to apply it. This allows one to use models of different complexity for describing the g.s. electron density, like the crude step-density model, or Thomas-Fermi and Kohn-Sham models. Consequently, we compare them and establish their influence on the quantitative results. In particular, we conclude that the ITFW g.s. electronic densities yield results in good agreement with the full KS-RPA calculations. This is of great importance for the applicability of the method, since for spheres with $N \geq 200$, self-consistent KS-RPA calculations are not technically feasible due to the increasing washing out of the electronic shell structure of the sphere. The step-density model has turned out to be quite useful in the characterization of bulk modes, as it magnifies the size-quantization effects while bearing the general features of the more realistic models.

We have separately analyzed the q and L dependences of the collective excitation energies. We conclude that surface-mode frequencies ω_L are q independent and that for each angular-momentum value different from zero there is only one surface mode. The volume modes are q quantized. For a fixed L value, one needs a second quantum index i that labels the bulk-mode frequency $\omega_{L,i}$ and determines its q_i-momentum value. The number of $q_i < q_c$ values increases with N and tends to a continuum when $N \to \infty$. As expected, for values of q larger than q_c, i.e., short excitation wavelengths, no collective modes are possible and the excitation energy tends to that of a quasifree electron.

It is worth discussing the meaning of the parameter q entering the definition of the external field. For small energies, the well-defined quantum number is the angular momentum L. The frequency ω_L of the mode is independent of q. For intermediate energies, bulk modes $\omega_{L,i}$ are excited predominantly. Thus, the longitudinal character of the excitation increases because of this fact and of the decreasing excitation probability of surface modes, which are of transverse character. In this intermediate energy region, the momenta q and L are partially good quantum numbers. Finally, for large energies, the spherical geometry is irrelevant, the q momentum is a well-defined quantum number, and the frequencies $\omega(q)$ are actually L independent.

For a plane wave representing a real photon, the response of the metallic sphere at intermediate energies is dominated by dipolar excitations and at large energies by

electron-hole excitations made possible by the energy exchange between this excitation and the sphere as a whole.

We have obtained a simple RPA dispersion relation for the infinite electron gas which includes exchange and correlation effects, generalizing the dispersion relation obtained by Lundqvist in the plasmon-pole approximation.[22]

We conclude that the q quantization is the origin of the oscillations in the scattering spectrum found by Batson[9] (see Fig. 7 of Ref. 9). In his experiment, he finds an oscillatory behavior of the scattering amplitude as a function of the radius of the sphere. It seems clear from our results that for a fixed momentum q, the scattering will be resonant for all the radii R such that qR corresponds to a peak in the response function. This already stems from the step-density hydrodynamical model. Here, we have shown that more realistic models also predict the same behavior.

Finally, recent experiments on electron-energy-loss spectroscopy carried out for K clusters[23] unambiguously show that for small values of q, the electronic response of these clusters is dominated by the surface-plasmon excitation. When q increases, the surface peak is washed out and a q-quantized volume mode is preferently excited (see Fig. 2 of Ref. 23). This behavior is in qualitative agreement with the results we have obtained for Na clusters (see for example our Fig. 5).

Note added in proof. Recent high-resolution electron-energy-loss spectrocopy measurements in aluminum carried out by Sprösser-Prou *et al.*[25] have been used by these authors to study the Al bulk-plasmon dispersion relation. Taking for Al $r_s=2.07$ a.u., Eq. (41) is able to reproduce their experimental results within a 6% error for all the measured q values.

ACKNOWLEDGMENTS

We would like to thank Angel Rubio for useful discussions. This work has been supported in part by the Comisión Asesora de Investigación Científica y Técnica (CAICyT), Spain under Grants Nos. PB85-0072-C02-00, AE87-0027, and PB84-0388-C04-03, and by the University of Barcelona- and the University of Valencia-University of the Balearic Islands exchange programs.

APPENDIX

In this Appendix we collect the formulas for m_1 and m_3 corresponding to $j_L(qr)Y_{L0}$ in the case of a step electron density n of radius R. We will denote by j_L the spherical Bessel function[24] $j_L(qR)$ and by $j'_L(qR)$ its derivative with respect to r evaluated at $r=R$. The quantities $\varepsilon_2^{cx}(n)$, $\varepsilon_2^{\rm corr}(n)$, and γ have been defined in the main text. We have

$$m_1=\frac{\hbar^2}{4m}\frac{nq^2R^3}{2L+1}[L(j_{L-1}^2-j_{L-2}j_L)+(L+1)(j_{L+1}^2-j_L j_{L+2})]\ , \tag{A1}$$

$$m_3(cx,\text{corr})=\tfrac{1}{4}\varepsilon_2^{cx,\text{corr}}(n)\left[\frac{\hbar^2}{m}\right]^2 q^2R^2[j_Lj'_L+q^2R(j_L^2-j_{L-1}j_{L+1})]\ , \tag{A2}$$

$$\begin{aligned}m_3(T)=\frac{1}{2}\left[\frac{\hbar^2}{m}\right]^3\Bigg[&\left[\frac{\gamma n^{5/3}}{3}+\frac{nq^2}{4}\right]\frac{q^2R^2}{2L+1}[L(j_{L-1}^2)'+(L+1)(j_{L+1}^2)']\\&+\frac{q^4\gamma n^{5/3}R^3}{2(2L+1)}[L(j_{L-1}^2-j_{L-2}j_L)+(L+1)(j_{L+1}^2-j_Lj_{L+2})]\\&+\frac{q^6nR^3}{8}(j_L^2-j_{L-1}j_{L+1})+\frac{q^4nR^2}{4}j_Lj'_L\Bigg]\ ,\end{aligned} \tag{A3}$$

$$m_3(C)=2\pi e^2\left[\frac{\hbar^2}{m}\right]^2 n^2R^3\left[\frac{q^2}{2}j_L^2-\frac{1}{2L+1}j_L'^2-\frac{q^2(2L+3)}{2(2L+1)}j_{L-1}j_{L+1}+\frac{2}{R}\frac{L}{2L+1}j_Lj'_L\right]\ . \tag{A4}$$

[1]W. A. de Heer, W. D. Knight, M. Y. Chou, and M. L. Cohen, in *Solid State Physics* edited by F. Seitz and D. Turnbull (Academic, New York, 1987), Vol. 40, p. 93.
[2]J. A. A. J. Perenboom, P. Wyder, and F. Meier, Phys. Rep. **78**, 173 (1981).
[3]M. J. Puska, R. M. Nieminen, and M. Manninen, Phys. Rev. B **31**, 3486 (1985).
[4]N. Barberán and J. Bausells, Phys. Rev. B **31**, 6354 (1985).
[5]W. Ekardt, Phys. Rev. B **31**, 6360 (1985).
[6]T. L. Ferrell and P. M. Echenique, Phys. Rev. Lett. **55**, 1526 (1985).
[7]R. Fuchs and F. Claro, Phys. Rev. B **35**, 3722 (1987).
[8]Ll. Serra, F. Garcias, M. Barranco, J. Navarro, C. Balbás, and A. Mañanes, Phys. Rev. B **39**, 8247 (1989).
[9]P. E. Batson, Surf. Sci. **156**, 720 (1985).
[10]R. Ruppin, Phys. Rev. B **11**, 2871 (1975).
[11]W. Ekardt, Phys. Rev. B **36**, 4483 (1987).
[12]Ll. Serra, F. Garcias, M. Barranco, J. Navarro, L. C. Balbás, A. Rubio, and A. Mañanes, J. Phys. Condens. Matter **1**, 10 391 (1989).
[13]O. Bohigas, A. M. Lane, and J. Martorell, Phys. Rep. **51**, 267 (1979).

[14]E. Lipparini and S. Stringari, Phys. Rep **175**, 103 (1989).
[15]G. Bertsch and W. Ekardt, Phys. Rev. B **32**, 7659 (1985).
[16]M. Brack, Phys. Rev. B **39**, 3533 (1989).
[17]J. Navarro and M. Barranco, Nucl. Phys. A **505**, 173 (1989).
[18]M. Casas and J. Martorell, Nucl. Phys. A **490**, 329 (1989).
[19]P. Gleissl, M. Brack, J. Meyer, and P. Quentin, Ann. Phys. (N.Y.) (to be published).
[20]S. Stringari, Ann. Phys. (N.Y.) **151**, 35 (1983).
[21]A. Rubio (private communication).
[22]B. I. Lundqvist, Phys. Status Solidi **32**, 273 (1969).
[23]A. vom Felde, J. Fink, and W. Ekardt, Phys. Rev. Lett. **61**, 2249 (1988).
[24]*Handbook of Mathematical Functions,* edited by M. Abramowitz and I. A. Stegun (Dover, New York, 1970).
[25]J. Sprösser-Prou, A. vom Felde, and J. Fink, Phys. Rev. B **40**, 5799 (1989).